Science

RESEARCH ARTI

Cite as: S. Hartweg *et al.*, *Science* 10.1126/science.adh0184 (2023).

Solvated dielectrons from optical excitation: An effective source of low-energy electrons

Sebastian Hartweg[1,2]*, Jonathan Barnes[3], Bruce L. Yoder[3], Gustavo A. Garcia[1], Laurent Nahon[1], Evangelos Miliordos[3,4], Ruth Signorell[3]*

[1]Synchrotron SOLEIL, L'Orme des Merisiers, Départementale 128, 91190 St Aubin, France. [2]Institute of Physics, University of Freiburg, Hermann-Herder-Straße 3a, 79104 Freiburg, Germany. [3]Department of Chemistry and Applied Biosciences, Laboratory of Physical Chemistry, ETH Zurich, Vladimir-Prelog-Weg 2, 8093 Zurich, Switzerland. [4]Department of Chemistry and Biochemistry, Auburn University, 179 Chemistry Building, Auburn, AL, USA.

*Corresponding author. Email: sebastian.hartweg@physik.uni-freiburg.de (S.H.); ruth.signorell@phys.chem.ethz.ch (R.S.)

Low-energy electrons dissolved in liquid ammonia or aqueous media are powerful reducing agents that promote challenging reduction reactions, but can also cause radiation damage to biological tissue. Knowledge of the underlying mechanistic processes remains incomplete, in particular with respect to the details and energetics of the electron transfer steps. Here, we show how ultraviolet (UV) photoexcitation of metal-ammonia clusters could be used to generate tunable low-energy electrons in situ. Specifically, we identified UV light-induced generation of spin-paired solvated dielectrons and their subsequent relaxation by an unconventional electron-transfer-mediated decay as an efficient low-energy electron source. The process is robust and straightforward to induce, with the prospect of improving our understanding of radiation damage and fostering mechanistic studies of solvated electron reduction reactions.

Unbound low-energy electrons are produced in liquids by ionizing radiation or arise as intermediates in chemical reactions. If their kinetic energy lies below the first electronic excitation threshold of the liquid, they are also referred to as subexcitation electrons. Being potent chemical reduction reagents, slow electrons are able to drive reactions in molecular solvents, such as liquid water and ammonia (*1*, *2*). Subexcitation electrons have been identified as important components in the chain of radiation chemistry in aqueous environments, for example causing severe damage to DNA molecules (*1*, *3*). Our understanding of these electron-induced reactions is still far from complete, in part due to the difficulty of performing controlled low-energy electron studies in liquids. Solvated electrons have been widely used as strong reducing agents in chemical synthesis. The most famous example is the Birch reduction, which relies on the high reducing power of solvated electrons of alkali metals dissolved in liquid ammonia (*2*, *4*). The conditions, however, are technically demanding and hazardous, which has prompted the search for alternative approaches. Even though substantial progress has been made in this direction (*5*–*7*), it proved challenging to find alternative approaches that can match the high reduction capability of the Birch reaction under milder conditions. Various Birch-type photoreduction pathways have been explored in this context (*5*–*7*), culminating in the discovery of a consecutive light-induced electron transfer catalytic cycle capable of generating highly reducing solvated electrons (*7*). Detailed mechanistic studies of such complex multicomponent systems remain challenging, highlighting the demand for simpler model systems to investigate individual steps. Reduction of aqueous carbon dioxide and nitrogen by solvated electrons was demonstrated using ultraviolet illumination of diamond as electron source (*8*, *9*). Comparable photoinduced electron transfer processes have not yet been reported for the conventional Birch system; i. e. alkali metal-ammonia solutions.

Here, we report a hitherto unknown light-induced electron transfer mechanism in alkali metal-ammonia solutions that efficiently produces low-energy electrons via the intermediate formation of a solvated dielectron. Composed of only a single solvent and solute, this system is exceptionally simple and thus amenable to fundamental studies of photoinduced electron transfers processes. In the mechanism we discovered, ultraviolet (UV) light promotes an electron from a valence orbital of the solvent molecules to the singly-occupied solvated electron orbital, generating a solvated spin-paired dielectron. The dielectron subsequently decays via an Electron-Transfer-Mediated Decay (ETMD) process. As key intermediates, dielectrons (also referred to as bipolarons) play the central part in this charge transfer process. Although there has been much progress in unravelling the nature of single (unpaired) solvated electrons (*10*–*21*), the same is not true for the dielectron, whose direct experimental observation has proven difficult. To date, insight into the characteristics of this elusive species mostly relies on theoretical studies (*10*, *21*–*25*). The diamagnetism observed experimentally in metal-ammonia solutions at higher metal concentration was explained by electron spin-pairing, although no definitive identification of the spin-paired species was possible (*10*, *15*, *26*).

Experimental evidence for hydrated dielectrons has also been found in radiolysis experiments (*27*) and in mass-spectrometric studies of water clusters anions (*23*). However, recent photoelectron studies on metal-ammonia solutions covering a wide range of metal concentrations failed to detect signatures specific to the dielectron in the experimental spectra (*24*, *28*).

Based on quantum chemical calculations, Larsen and Schwartz have suggested possible experimental procedures to create detectable amounts of metastable dielectrons by capturing a second electron in the cavity of a pre-existing single solvated electron (*21*). Pulsed radiolysis experiments and time-delayed multi-pulse laser schemes were proposed. Inspired by their work, we have developed an alternative UV photoexcitation - photoelectron detection method that can not only generate high yields of metastable dielectrons, but also detect them via a unique photoelectron signature. The key to selective detection of dielectrons is the special ETMD process, effectively replacing the pump-probe detection steps in the schemes suggested in ref. (*21*). ETMD and ICD (Intermolecular Coulombic Decay), i. e. non-local decay processes of electronically excited species, were first predicted theoretically (*29–31*) before being observed experimentally in the soft X-ray range (*32–34*). ETMD processes accessible by UV light excitation offer new perspectives for the practical use of such non-local decay processes. Here, we show how slow electrons were produced in a straightforward way by this surprising UV-pumped dielectron-ETMD process. The discovered slow electron formation pathway could play a role in mechanistic studies of radiation chemistry and solvated electron reduction reactions.

Photoelectron spectroscopy

UV light-induced generation of low-energy electrons was directly probed in sodium-doped ammonia clusters ($Na(NH_3)_n$) using double-imaging photoelectron-photoion coincidence spectroscopy at the DESIRS VUV beamline of the Synchrotron SOLEIL (see supplementary materials, sections S1and S2, and (*35*)). Coincidence spectroscopy provided cluster-size resolved photoelectron spectra (PES) and images (Fig. 1).The experiments were complemented by quantum chemical calculations of the ground and electronically excited states of the clusters treating electron correlation in terms of Møller-Plesset and Coupled Cluster theory ((*36*, *37*); sections S4 to S8). The combined approach allowed us to identify the UV light-induced generation of solvated, spin-paired dielectrons and their subsequent ETMD as the source of low-energy electrons. The mechanism we discovered also explains the dominance of this process over a broad UV wavelength range.

Figure 1A (blue to green traces) shows representative PES of $Na(NH_3)_n$ clusters acquired at different UV photon energies $h\nu$ (see section S3 for PES of larger clusters). Higher electron binding energies (eBE) correspond to lower electron kinetic energies ($E_{kin} = h\nu$-eBE; fig. S2). PES recorded at photon energies below 5.5 eV (dark blue traces in Fig. 1A) consist of a single, narrow low-eBE band (feature "F1") (*17*), and PES recorded at 9.9 eV (green traces) consist of a single, high-eBE band (feature "F2"). At intermediate photon energies (5.5 eV< $h\nu$ <9.9 eV), the PES are dominated by an unexpectedly broad distribution of low-kinetic energy electrons (E_{kin} < 6 eV; fig. S2), with increasing electron abundance toward zero kinetic energy (feature "F3" in the light blue, orange and red traces). Supported by quantum chemical calculations (sections S4 to S8), the observation of the three distinct features F1, F2 and F3 points to three distinct pathways of electron formation (Fig. 2), which can be turned on and off selectively by the choice of UV photon energy.

Direct photoionization of solvated electrons and solute molecules

The sharp F1 band results from direct photoionization of the solvated sodium 3s electron (Φ_{solv} in Fig. 2D, (*17–19*, *38*)) corresponding to the transition from the electronic ground state ^2X of the neutral cluster to the electronic ground state $^1X^+$ of the cationic cluster (Fig. 2A). The high symmetry of Φ_{solv} is reflected in the pronounced anisotropic photoelectron distributions (Fig. 1B at $h\nu$ = 5.5 eV, (*17*)). The coincidence study directly provided cluster size-resolved vertical eBEs in good agreement with ab initio calculations (tables S1 and S2). The vertical eBE decreases systematically from 4.3 eV for $Na(NH_3)$ to ~2.6 eV for $Na(NH_3)_{10}$, where it converges with respect to cluster size (figs. S3 and S4). The cluster size-resolved eBE values improve and extend previous data obtained from PES of cluster ensembles and photoion studies (*17*, *18*).

A different pathway of electron formation dominates at photon energies above the lowest ionization energy of the NH_3 solvent molecules (Fig. 1A, green trace at $h\nu$ = 9.9 eV; (*39*)). Here, ionization occurs mainly via the removal of an electron from the highest occupied molecular orbital (HOMO) of the $(NH_3)_n$ solvent shell, Φ_L (Fig. 2E), instead of ionization from the HOMO of the entire $Na(NH_3)_n$ cluster, Φ_{solv}. The assignment of the F2 band to ionization from Φ_L is corroborated by the good agreement with the PES of pure liquid ammonia (*40*) and ammonia clusters (*39*), and by the fact that the PES of $Na(NH_3)_n$ clusters and bare $(NH_3)_n$ clusters are very similar (Fig. 1A, green and black traces, respectively). The F1 band is missing at hν= 9.9 eV because of the higher ionization probability from Φ_L compared with that from Φ_{solv} combined with a large increase of the total number of photoelectrons (direct ionization of NH_3 molecules) and the limited dynamic range of the coincidence detection. The almost identical PES for $Na(NH_3)_n$ and bare $(NH_3)_n$ clusters imply that the electronic structure of the NH_3 solvent molecules is only slightly affected by the presence of the Na^+ cation and the solvated electron. In stark contrast to the PES, the relaxation

dynamics after direct photoionization critically depends on the absence ($(NH_3)_n$) or presence ($Na(NH_3)_n$) of a solvated electron. Relaxation of bare $(NH_3)_n^+$ cluster ions occurs via proton transfer between neighboring NH_3 molecules, and the release of an $NH_2^\bullet$ radical from the cluster: $(NH_3)_n + h\nu = (NH_3)_{n-1}H^+ + NH_2^\bullet + e_{ph}^-$ (*41*). Thus, mass spectra of undoped ammonia clusters consist of protonated cluster signals $(NH_3)_{n-1}H^+$ (major mass peaks in Fig. 1C). This ultrafast relaxation pathway via proton transfer is well-known to occur in various hydrogen bonded systems (*41*). The proton transfer is completely suppressed in the presence of a solvated electron by the fast electron transfer from Φ_{solv} to Φ_L (Fig. 3B and section S8). Here, the mass spectra show intact cluster ion signals $Na(NH_3)_n^+$ (minor mass peaks in Fig. 1C) instead of ion signals of protonated clusters. Albeit ionization occurs from the same ammonia orbital (Φ_L) in neat and Na-doped clusters, the presence of the solvated electron opens an unexpected relaxation pathway in $Na(NH_3)_n$ that is faster than the proton transfer pathway. We propose that relaxation of $Na(NH_3)_n^+$ clusters occurs via initial ultrafast electron transfer from the delocalized Φ_{solv} orbital to the localized Φ_L vacancy formed by photoionization (Fig. 2B), with subsequent energy dissipation via internal conversion. The electron hopping between Φ_{solv} and the Φ_L vacancy corresponds to a transition from the first electronically excited $^1a^+$ state of the cluster cation to its $^1x^+$ ground state. This electron transfer is analogous to the first step of a Birch reduction, in which a solvated electron transfers to an unoccupied molecular orbital.

Low-energy electron formation via decay of dielectrons

Even more intriguing with respect to the formation of reducing electrons is the mechanism that occurs after photoexcitation with photons of ~5.5 to 8 eV energy (wavelength ~225 to 155 nm). Here, PES are dominated by the broad F3 feature (Fig. 1A). This band corresponds to a broad distribution of low-kinetic energy electrons, with increasing electron abundance toward zero kinetic energy (maximum eBE; fig. S2) and isotropic angular distribution (Fig. 1B, left). This behavior is fully consistent with the excitation of a dielectron state which autoionizes by ETMD (Fig. 2C). Conceivable alternative mechanisms to explain the origin of the F3 feature are assessed in section S8 in detail. Since they prove to be inconsistent with our experimental observations, we do not discuss them here further. The dielectron/ETMD mechanism producing the F3 electrons is visualized in Fig. 2C. Direct ionization from the ammonia HOMO Φ_L, responsible for the F2 band, is not possible at these lower photon energies. Instead, photoexcitation promotes an electron from Φ_L to the singly occupied, delocalized solvated electron orbital Φ_{solv} to form a metastable, solvated spin-paired dielectron. This unusual electronically excited dielectron state, ^2A, is characterized by a doubly occupied Φ_{solv} orbital and a vacancy in the Φ_L orbital of the solvation shell, in agreement with ab initio calculations (Fig. 3 and sections S4 and S5). Regarding the difference of this dielectron compared with the ground state dielectron species postulated in metal-ammonia solutions (*10*), we refer the reader to section S8. The ^2A state lies above the $^1x^+$ electronic ground state of the cation and autoionizes via a unique version of ETMD (Fig. 2C): One of the two delocalized electrons in Φ_{solv} transfers to the solvation shell where it localizes in the ammonia Φ_L vacancy. Concurrent with this transfer, the second electron is ejected with low kinetic energy (e^-_{ETMD}) and detected in the PES as part of the F3 band (Fig. 1A). The broad kinetic energy distribution of the resulting photoelectrons reflects the concerted progress of photoelectron ejection and electron transfer during the ETMD (see discussion of Fig. 3). This UV light-induced-ETMD process offers a straightforward way to generate high yields of dielectrons, and to distinguish them (F3 band) from the always accompanying single solvated electrons (F1 band) (*21*, *24*, *28*). Compared with previously reported ETMD processes (*30*–*32*, *34*, *42*, *43*), this ETMD is distinctive in two aspects: The electron transfer goes hand in hand with a considerable spatial contraction of the electron wavefunction, and it is initiated by exceptionally low photon energies in the UV range. The former might enhance the efficiency of the electron transfer, the latter makes ETMD more amenable to applications.

Figure 3 shows computational results of the potential energy profiles (PEPs) along the one-dimensional relaxation path of the neutral dielectron state (red), following vertical photoexcitation from the neutral ground state (black). The large difference between the equilibrium geometries of electronic ground and dielectron state imply a broad Franck-Condon progression in the photoexcitation spectrum, which makes the dielectron state accessible over a broad range of UV photon energies. The PEP of the cationic state (blue) intersects the PEP of the dielectron state just before its minimum, A_{min}, has been reached. The selected vibrational wavefunctions (dashed curves) of the dielectron state and the cationic state highlight the many possibilities along the relaxation path for ETMD processes to occur (section S4 and S5), which are reflected in the broad kinetic energy distribution of the $e^-_{ETMD,}$ constituting the F3 band in Fig. 1A. In terms of a time-dependent wave packet picture, an increased hopping probability near the intersection with the cationic ground state PEP offers a plausible explanation for the observed preference of the e^-_{ETMD} toward zero kinetic energies (see discussion of fig. S2 in sections S3 and S8). For all photon energies, the sharp cut-off of the F3 feature (Fig. 1A) is therefore located at a binding energy corresponding to the photon energy. The observed high yield of e^-_{ETMD} is consistent with a high photoexcitation probability from the neutral ground state to delocalized dielectron states, and a high autoionization probability via ETMD (section S9).

Figure 4 shows the relative electron yields of the F3 band for selected cluster sizes at three different photoexcitation energies. Several essential insights emerge from these results. ETMD dominates electron formation over a broad range of photoexcitation energies, extending from the near to the far UV. It is largely insensitive to the specific UV photon energy. Except for the smallest clusters ($n \leq 2$), ETMD does not depend on the cluster size either (see figs. S3 and S4 for larger clusters). The stability of the ETMD process with respect to changes of the system size was also confirmed by calculations, so that autoionization via solvated dielectrons should persist in bulk solutions (section S6). Moreover, the phenomenon exhibits some robustness to chemical changes. For example, replacing sodium with lithium had little effect (section S6). Theoretical assessment of solvent exchange proved to be more challenging due to competing relaxation channels (section S7). For solvents hosting solvated electrons, the formation of slow electrons from a transient dielectron state via ETMD generally appears to be an important channel.

Conclusions

What are the possible implications of this hitherto unknown slow electron formation pathway? ICD and ETMD have been discussed as in-situ sources of low-energy electrons, with the caveat that high-energy photon sources are generally required to trigger these processes. The present ETMD process offers the possibility to use conventional UV lamps in the near to far UV range. By controlling the photon energy the maximum electron kinetic energy can be tuned across the subexcitation range. This could be exploited for systematic energy-dependent mechanistic studies relevant to radiation chemistry and radiation damage in biological tissues. Given that broadband UV lamps can be used for in-situ generation of high yields of low-energy electrons, the discovery of the dielectron-ETMD mechanism might also be of practical relevance to electron reduction reactions. It is conceivable that reduction reactions with solvated electrons are photo-enhanced by the dielectron-ETMD mechanism, as the more highly energized ETMD electrons could overcome reaction barriers unsurmountable to common solvated electrons. It would be intriguing to study the energy-dependent activity of the solvated electron as a reducing agent by tuning the energy of the ETMD electron. Future investigations of the dynamics of dielectron/ETMD process after UV photoexcitation might even hold the prospect of discovering new reaction pathways.

REFERENCES AND NOTES

1. B. C. Garrett, D. A. Dixon, D. M. Camaioni, D. M. Chipman, M. A. Johnson, C. D. Jonah, G. A. Kimmel, J. H. Miller, T. N. Rescigno, P. J. Rossky, S. S. Xantheas, S. D. Colson, A. H. Laufer, D. Ray, P. F. Barbara, D. M. Bartels, K. H. Becker, K. H. Bowen Jr., S. E. Bradforth, I. Carmichael, J. V. Coe, L. R. Corrales, J. P. Cowin, M. Dupuis, K. B. Eisenthal, J. A. Franz, M. S. Gutowski, K. D. Jordan, B. D. Kay, J. A. Laverne, S. V. Lymar, T. E. Madey, C. W. McCurdy, D. Meisel, S. Mukamel, A. R. Nilsson, T. M. Orlando, N. G. Petrik, S. M. Pimblott, J. R. Rustad, G. K. Schenter, S. J. Singer, A. Tokmakoff, L.-S. Wang, C. Wettig, T. S. Zwier, Role of water in electron-initiated processes and radical chemistry: Issues and scientific advances. *Chem. Rev.* **105**, 355–390 (2005). doi:10.1021/cr030453x Medline
2. P. W. Rabideau, Z. Marcinow, in *Organic Reactions*, L. A. Paquette, Ed. (Wiley, 1992), pp. 1–334.
3. E. Alizadeh, L. Sanche, Precursors of solvated electrons in radiobiological physics and chemistry. *Chem. Rev.* **112**, 5578–5602 (2012). doi:10.1021/cr300063r Medline
4. A. J. Birch, 117. Reduction by dissolving metals. Part I. *J. Chem. Soc.* **1944**, 430–436 (1944).
5. B. K. Peters, K. X. Rodriguez, S. H. Reisberg, S. B. Beil, D. P. Hickey, Y. Kawamata, M. Collins, J. Starr, L. Chen, S. Udyavara, K. Klunder, T. J. Gorey, S. L. Anderson, M. Neurock, S. D. Minteer, P. S. Baran, Scalable and safe synthetic organic electroreduction inspired by Li-ion battery chemistry. *Science* **363**, 838–845 (2019). doi:10.1126/science.aav5606 Medline
6. A. Chatterjee, B. König, Birch-type photoreduction of arenes and heteroarenes by sensitized electron transfer. *Angew. Chem. Int. Ed.* **58**, 14289–14294 (2019). doi:10.1002/anie.201905485 Medline
7. J. P. Cole, D.-F. Chen, M. Kudisch, R. M. Pearson, C.-H. Lim, G. M. Miyake, Organocatalyzed Birch reduction driven by visible light. *J. Am. Chem. Soc.* **142**, 13573–13581 (2020). doi:10.1021/jacs.0c05899 Medline
8. L. Zhang, D. Zhu, G. M. Nathanson, R. J. Hamers, Selective photoelectrochemical reduction of aqueous CO_2 to CO by solvated electrons. *Angew. Chem. Int. Ed.* **53**, 9746–9750 (2014). doi:10.1002/anie.201404328 Medline
9. D. Zhu, L. Zhang, R. E. Ruther, R. J. Hamers, Photo-illuminated diamond as a solid-state source of solvated electrons in water for nitrogen reduction. *Nat. Mater.* **12**, 836–841 (2013). doi:10.1038/nmat3696 Medline
10. E. Zurek, P. P. Edwards, R. Hoffmann, A molecular perspective on lithium-ammonia solutions. *Angew. Chem. Int. Ed.* **48**, 8198–8232 (2009). doi:10.1002/anie.200900373 Medline
11. R. M. Young, D. M. Neumark, Dynamics of solvated electrons in clusters. *Chem. Rev.* **112**, 5553–5577 (2012). doi:10.1021/cr300042h Medline
12. J. M. Herbert, M. P. Coons, The hydrated electron. *Annu. Rev. Phys. Chem.* **68**, 447–472 (2017). doi:10.1146/annurev-physchem-052516-050816 Medline
13. P. Vöhringer, Ultrafast dynamics of electrons in ammonia. *Annu. Rev. Phys. Chem.* **66**, 97–118 (2015). doi:10.1146/annurev-physchem-040214-121228 Medline
14. O. Marsalek, F. Uhlig, J. VandeVondele, P. Jungwirth, Structure, dynamics, and reactivity of hydrated electrons by ab initio molecular dynamics. *Acc. Chem. Res.* **45**, 23–32 (2012). doi:10.1021/ar200062m Medline
15. P. P. Edwards, Magnetic resonance studies of alkali metals in nonaqueous solvents. *J. Phys. Chem.* **88**, 3772–3780 (1984). doi:10.1021/j150661a019
16. D. Luckhaus, Y. I. Yamamoto, T. Suzuki, R. Signorell, Genuine binding energy of the hydrated electron. *Sci. Adv.* **3**, e1603224 (2017). doi:10.1126/sciadv.1603224 Medline
17. A. H. C. West, B. L. Yoder, D. Luckhaus, C.-M. Saak, M. Doppelbauer, R. Signorell, Angle-resolved photoemission of solvated electrons in sodium-doped clusters. *J. Phys. Chem. Lett.* **6**, 1487–1492 (2015). doi:10.1021/acs.jpclett.5b00477 Medline
18. T. Zeuch, U. Buck, Sodium doped hydrogen bonded clusters: Solvated electrons and size selection. *Chem. Phys. Lett.* **579**, 1–10 (2013). doi:10.1016/j.cplett.2013.06.011
19. A. O. Gunina, A. I. Krylov, Probing electronic wave functions of sodium-doped clusters: Dyson orbitals, anisotropy parameters, and ionization cross-sections. *J. Phys. Chem. A* **120**, 9841–9856 (2016). doi:10.1021/acs.jpca.6b10098 Medline
20. C. P. Schulz, A. Scholz, I. V. Hertel, Ultrafast energy redistribution in photoexcited sodium-ammonia clusters. *Isr. J. Chem.* **44**, 19–25 (2004). doi:10.1560/TEY2-WJ8Q-LMFT-U2V7
21. R. E. Larsen, B. J. Schwartz, Full configuration interaction computer simulation study of the thermodynamic and kinetic stability of hydrated dielectrons. *J. Phys. Chem. B* **110**, 1006–1014 (2006). doi:10.1021/jp0546453 Medline
22. G. J. Martyna, Z. Deng, M. L. Klein, Quantum simulation studies of singlet and triplet bipolarons in liquid ammonia. *J. Chem. Phys.* **98**, 555–563 (1993). doi:10.1063/1.464650

23. R. N. Barnett, R. Giniger, O. Cheshnovsky, U. Landman, Dielectron attachment and hydrogen evolution reaction in water clusters. *J. Phys. Chem. A* **115**, 7378–7391 (2011). doi:10.1021/jp201560n Medline
24. T. Buttersack, P. E. Mason, R. S. McMullen, H. C. Schewe, T. Martinek, K. Brezina, M. Crhan, A. Gomez, D. Hein, G. Wartner, R. Seidel, H. Ali, S. Thürmer, O. Marsalek, B. Winter, S. E. Bradforth, P. Jungwirth, Photoelectron spectra of alkali metal-ammonia microjets: From blue electrolyte to bronze metal. *Science* **368**, 1086–1091 (2020). doi:10.1126/science.aaz7607 Medline
25. M. Mauksch, S. B. Tsogoeva, Spin-paired solvated electron couples in alkali-ammonia systems. *Phys. Chem. Chem. Phys.* **20**, 27740–27744 (2018). doi:10.1039/C8CP05058A Medline
26. U. Schindewolf, M. Werner, Thermodynamics of sodium-ammonia solutions. *J. Phys. Chem.* **84**, 1123–1129 (1980). doi:10.1021/j100447a009
27. K. H. Schmidt, D. M. Bartels, Lack of ionic strength effect in the recombination of hydrated electrons: $(e^-)_{aq} + (e^-)_{aq} \rightarrow 2(OH^-) + H_2$. *Chem. Phys.* **190**, 145–152 (1995). doi:10.1016/0301-0104(94)00332-5
28. S. Hartweg, A. H. C. West, B. L. Yoder, R. Signorell, Metal transition in sodium–ammonia nanodroplets. *Angew. Chem. Int. Ed.* **55**, 12347–12350 (2016). doi:10.1002/anie.201604282 Medline
29. L. S. Cederbaum, J. Zobeley, F. Tarantelli, Giant Intermolecular Decay and Fragmentation of Clusters. *Phys. Rev. Lett.* **79**, 4778–4781 (1997). doi:10.1103/PhysRevLett.79.4778
30. J. Zobeley, R. Santra, L. S. Cederbaum, Electronic decay in weakly bound heteroclusters: Energy transfer versus electron transfer. *J. Chem. Phys.* **115**, 5076–5088 (2001). doi:10.1063/1.1395555
31. A. Ghosh, L. S. Cederbaum, K. Gokhberg, Signature of the neighbor's quantum nuclear dynamics in the electron transfer mediated decay spectra. *Chem. Sci.* **12**, 9379–9385 (2021). doi:10.1039/D1SC01478A Medline
32. K. Sakai, S. Stoychev, T. Ouchi, I. Higuchi, M. Schöffler, T. Mazza, H. Fukuzawa, K. Nagaya, M. Yao, Y. Tamenori, A. I. Kuleff, N. Saito, K. Ueda, Electron-transfer-mediated decay and interatomic Coulombic decay from the triply ionized states in argon dimers. *Phys. Rev. Lett.* **106**, 033401 (2011). doi:10.1103/PhysRevLett.106.033401 Medline
33. T. Jahnke, A. Czasch, M. S. Schöffler, S. Schössler, A. Knapp, M. Käsz, J. Titze, C. Wimmer, K. Kreidi, R. E. Grisenti, A. Staudte, O. Jagutzki, U. Hergenhahn, H. Schmidt-Böcking, R. Dörner, Experimental observation of interatomic coulombic decay in neon dimers. *Phys. Rev. Lett.* **93**, 163401 (2004). doi:10.1103/PhysRevLett.93.163401 Medline
34. T. Jahnke, U. Hergenhahn, B. Winter, R. Dörner, U. Frühling, P. V. Demekhin, K. Gokhberg, L. S. Cederbaum, A. Ehresmann, A. Knie, A. Dreuw, Interatomic and intermolecular Coulombic decay. *Chem. Rev.* **120**, 11295–11369 (2020). doi:10.1021/acs.chemrev.0c00106 Medline
35. X. Tang, G. A. Garcia, J.-F. Gil, L. Nahon, Vacuum upgrade and enhanced performances of the double imaging electron/ion coincidence end-station at the vacuum ultraviolet beamline DESIRS. *Rev. Sci. Instrum.* **86**, 123108 (2015). doi:10.1063/1.4937624 Medline
36. R. J. Bartlett, J. D. Watts, S. A. Kucharski, J. Noga, Non-iterative fifth-order triple and quadruple excitation energy corrections in correlated methods. *Chem. Phys. Lett.* **165**, 513–522 (1990). doi:10.1016/0009-2614(90)87031-L
37. K. Raghavachari, G. W. Trucks, J. A. Pople, M. Head-Gordon, A fifth-order perturbation comparison of electron correlation theories. *Chem. Phys. Lett.* **157**, 479–483 (1989). doi:10.1016/S0009-2614(89)87395-6
38. I. R. Ariyarathna, F. Pawłowski, J. V. Ortiz, E. Miliordos, Molecules mimicking atoms: Monomers and dimers of alkali metal solvated electron precursors. *Phys. Chem. Chem. Phys.* **20**, 24186–24191 (2018). doi:10.1039/C8CP05497E Medline
39. A. H. C. West, B. L. Yoder, R. Signorell, Size-dependent velocity map photoelectron imaging of nanosized ammonia aerosol particles. *J. Phys. Chem. A* **117**, 13326–13335 (2013). doi:10.1021/jp406313a Medline
40. T. Buttersack, P. E. Mason, R. S. McMullen, T. Martinek, K. Brezina, D. Hein, H. Ali, C. Kolbeck, C. Schewe, S. Malerz, B. Winter, R. Seidel, O. Marsalek, P. Jungwirth, S. E. Bradforth, Valence and Core-Level X-ray Photoelectron Spectroscopy of a Liquid Ammonia Microjet. *J. Am. Chem. Soc.* **141**, 1838–1841 (2019). doi:10.1021/jacs.8b10942 Medline
41. F. Dong, S. Heinbuch, J. J. Rocca, E. R. Bernstein, Dynamics and fragmentation of van der Waals clusters: $(H_2O)_n$, $(CH_3OH)_n$, and $(NH_3)_n$ upon ionization by a 26.5 eV soft x-ray laser. *J. Chem. Phys.* **124**, 224319 (2006). doi:10.1063/1.2202314 Medline
42. I. Unger, R. Seidel, S. Thürmer, M. N. Pohl, E. F. Aziz, L. S. Cederbaum, E. Muchová, P. Slavíček, B. Winter, N. V. Kryzhevoi, Observation of electron-transfer-mediated decay in aqueous solution. *Nat. Chem.* **9**, 708–714 (2017). doi:10.1038/nchem.2727 Medline
43. L. Ben Ltaief, M. Shcherbinin, S. Mandal, S. R. Krishnan, R. Richter, T. Pfeifer, M. Bauer, A. Ghosh, M. Mudrich, K. Gokhberg, A. C. LaForge, Electron transfer mediated decay of alkali dimers attached to He nanodroplets. *Phys. Chem. Chem. Phys.* **22**, 8557–8564 (2020). doi:10.1039/D0CP00256A Medline
44. S. Hartweg, J. Barnes, B. L. Yoder, G. A. Garcia, L. Nahon, E. Miliordos, R. Signorell, Solvated dielectrons from optical excitation: An effective source of low-energy electrons, data collection, ETH Zürich Research Collection (2023); https://doi.org/10.3929/ethz-b-000611963.
45. G. A. Garcia, B. K. Cunha de Miranda, M. Tia, S. Daly, L. Nahon, DELICIOUS III: A multipurpose double imaging particle coincidence spectrometer for gas phase vacuum ultraviolet photodynamics studies. *Rev. Sci. Instrum.* **84**, 053112 (2013). doi:10.1063/1.4807751 Medline
46. L. Nahon, N. de Oliveira, G. A. Garcia, J.-F. Gil, B. Pilette, O. Marcouillé, B. Lagarde, F. Polack, DESIRS: A state-of-the-art VUV beamline featuring high resolution and variable polarization for spectroscopy and dichroism at SOLEIL. *J. Synchrotron Radiat.* **19**, 508–520 (2012). doi:10.1107/S0909049512010588 Medline
47. B. L. Yoder, A. H. C. West, B. Schläppi, E. Chasovskikh, R. Signorell, A velocity map imaging photoelectron spectrometer for the study of ultrafine aerosols with a table-top VUV laser and Na-doping for particle sizing applied to dimethyl ether condensation. *J. Chem. Phys.* **138**, 044202 (2013). doi:10.1063/1.4788620 Medline
48. G. A. Garcia, L. Nahon, I. Powis, Two-dimensional charged particle image inversion using a polar basis function expansion. *Rev. Sci. Instrum.* **75**, 4989–4996 (2004). doi:10.1063/1.1807578
49. C. Nitsch, C. P. Schulz, A. Gerber, W. Zimmermann-Edling, I. V. Hertel, Photoionization studies of free sodium ammonia clusters. *Z. Phys. D Atoms Mol. Clust.* **22**, 651–658 (1992). doi:10.1007/BF01426368
50. I. V. Hertel IV, C. Hüglin, C. Nitsch, C. P. Schulz, Photoionization of $Na(NH_3)_n$ and $Na(H_2O)_n$ clusters: A step towards the liquid phase? *Phys. Rev. Lett.* **67**, 1767–1770 (1991). doi:10.1103/PhysRevLett.67.1767 Medline
51. T. H. Dunning Jr., Gaussian basis sets for use in correlated molecular calculations. I. The atoms boron through neon and hydrogen. *J. Chem. Phys.* **90**, 1007–1023 (1989). doi:10.1063/1.456153
52. R. A. Kendall, T. H. Dunning Jr., R. J. Harrison, Electron Affinities of the First-row Atoms Revisited. Systematic Basis Sets and Wave Functions. *J. Chem. Phys.* **96**, 6796–6806 (1992). doi:10.1063/1.462569
53. M. J. Frisch, G. W. Trucks, H. B. Schlegel, G. E. Scuseria, M. A. Robb, J. R. Cheeseman, G. Scalmani, V. Barone, G. A. Petersson, H. Nakatsuji, X. Li, M. Caricato, A. V. Marenich, J. Bloino, B. G. Janesko, R. Gomperts, B. Mennucci, H. P. Hratchian, J. V. Ortiz, A. F. Izmaylov, J. L. Sonnenberg, D. Williams-Young, F. Ding, F. Lipparini, F. Egidi, J. Goings, B. Peng, A. Petrone, T. Henderson, D. Ranasinghe, V. G. Zakrzewski, J. Gao, N. Rega, G. Zheng, W. Liang, M. Hada, M. Ehara, K. Toyota, R. Fukuda, J. Hasegawa, M. Ishida, T. Nakajima, Y. Honda, O. Kitao, H. Nakai, T. Vreven, K. Throssell, J. A. Montgomery Jr., J. E. Peralta, F. Ogliaro, M. J. Bearpark, J. J. Heyd, E. N. Brothers, K. N. Kudin, V. N. Staroverov, T. A. Keith, R. Kobayashi, J. Normand, K. Raghavachari, A. P. Rendell, J. C. Burant, S. S. Iyengar, J. Tomasi, M. Cossi, J. M. Millam, M. Klene, C. Adamo, R. Cammi, J. W. Ochterski, R. L. Martin, K. Morokuma, O. Farkas, J. B. Foresman, D. J. Fox, Gaussian 16, revision B.01 (Gaussian Inc., 2016).
54. H.-J. Werner, P. J. Knowles, P. Celani, W. Györffy, A. Hesselmann, D. Kats, G. Knizia, A. Köhn, T. Korona, D. Kreplin, R. Lindh, Q. Ma, F. R. Manby, A. Mitrushenkov, G. Rauhut, M. Schütz, K. R. Shamasundar, T. B. Adler, R. D. Amos, S. J. Bennie, A. Bernhardsson, A. Berning, J. A. Black, P. J. Bygrave, R. Cimiraglia, D. L. Cooper, D. Coughtrie, M. J. O. Deegan, A. J. Dobbyn, K. Doll, M. Dornbach, F. Eckert, S. Erfort, E. Goll, C. Hampel, G. Hetzer, J. G. Hill, M. Hodges, T. Hrenar, G. Jansen, C. Köppl, C. Kollmar, S. J. R. Lee, Y. Liu, A. W. Lloyd, R. A. Mata, A. J. May, B. Mussard, S. J. McNicholas, W. Meyer, T. F. Miller III, M. E. Mura, A. Nicklass, D. P. O'Neill, P. Palmieri, D. Peng, K. A. Peterson, K. Pflüger, R. Pitzer, I. Polyak, M. Reiher, J. O. Richardson, J. B. Robinson, B. Schröder, M. Schwilk, T. Shiozaki, M.

Sibaev, H. Stoll, A. J. Stone, R. Tarroni, T. Thorsteinsson, J. Toulouse, M. Wang, M. Welborn, B. Ziegler, MOLPRO, version 2015.1, a package of ab initio programs (2015); https://www.molpro.net.
55. I. R. Ariyarathna, N. M. S. Almeida, E. Miliordos, Stability and Electronic Features of Calcium Hexa-, Hepta-, and Octa-Coordinated Ammonia Complexes: A First-Principles Study. *J. Phys. Chem. A* **123**, 6744–6750 (2019). doi:10.1021/acs.jpca.9b04966 Medline
56. I. R. Ariyarathna, S. N. Khan, F. Pawłowski, J. V. Ortiz, E. Miliordos, Aufbau Rules for Solvated Electron Precursors: $Be(NH_3)_4^{0,\pm}$ Complexes and Beyond. *J. Phys. Chem. Lett.* **9**, 84–88 (2018). doi:10.1021/acs.jpclett.7b03000 Medline
57. Miliordos Research Group, Rovib (Auburn University, 2016); https://auburn.edu/cosam/faculty/chemistry/miliordos/my_lab/page7.htm.
58. B. Baranyi, L. Turi, Excess electron solvation in ammonia clusters. *J. Chem. Phys.* **151**, 204304 (2019). doi:10.1063/1.5123790 Medline
59. B. Baranyi, L. Turi, Ab Initio Molecular Dynamics Simulations of Solvated Electrons in Ammonia Clusters. *J. Phys. Chem. B* **124**, 7205–7216 (2020). doi:10.1021/acs.jpcb.0c03908 Medline
60. H. M. Grubb, J. F. Chittum, H. Hunt, Liquid Ammonia as a Solvent. VI. The Dielectric Constant of Liquid Ammonia. *J. Am. Chem. Soc.* **58**, 776 (1936). doi:10.1021/ja01296a026
61. C. Steinbach, U. Buck, Reaction and solvation of sodium in hydrogen bonded solvent clusters. *Phys. Chem. Chem. Phys.* **7**, 986–990 (2005). doi:10.1039/b419325n Medline
62. K. Gokhberg, A. B. Trofimov, T. Sommerfeld, L. S. Cederbaum, Ionization of metal atoms following valence-excitation of neighbouring molecules. *Europhys. Lett.* **72**, 228–234 (2005). doi:10.1209/epl/i2005-10227-7

ACKNOWLEDGMENTS

We are grateful to D. Stapfer, M. Steger and J.-F. Gil for technical support, and to the general staff of SOLEIL for providing beamtime under project 20200627 and 99210131. EM acknowledges ETH Zurich and the United States National Science Foundation for a guest professorship, and SH acknowledges support by the Deutsche Forschungsgemeinschaft (DFG, RTG 2717). **Funding:** This project has received funding from the European Union's Horizon 2020 research and innovation program from the European Research Council under grant agreement 786636, the Swiss National Science Foundation (project 200020_200306), and the United States National Science Foundation (Grant No. CHE-1940456).
Author contributions: Conceptualization: SH, RS. Methodology: SH, BY, GG, LN, EM, RS. Investigation: SH, JB, BY, GG, LN, EM. Visualization: SH, EM, RS. Funding acquisition: EM, RS. Project administration: SH, RS. Supervision: LN, RS. Writing – original draft: SH, EM, RS. Writing – review & editing: SH, JB, BY, GG, LN, EM, RS. **Competing interests:** The authors declare no conflict of interest. **Data and materials availability:** All data that reproduce the analyses are available in a data repository (*44*). All (other) data needed to evaluate the conclusions in the paper are present in the paper or the supplementary materials.

SUPPLEMENTARY MATERIALS

science.org/doi/10.1126/science.adh0184
Supplementary Text
Figs. S1 to S11
Tables S1 to S8
References (*45*–*62*)

Submitted 6 February 2023; accepted 12 May 2023
Published online 25 May 2023
10.1126/science.adh0184

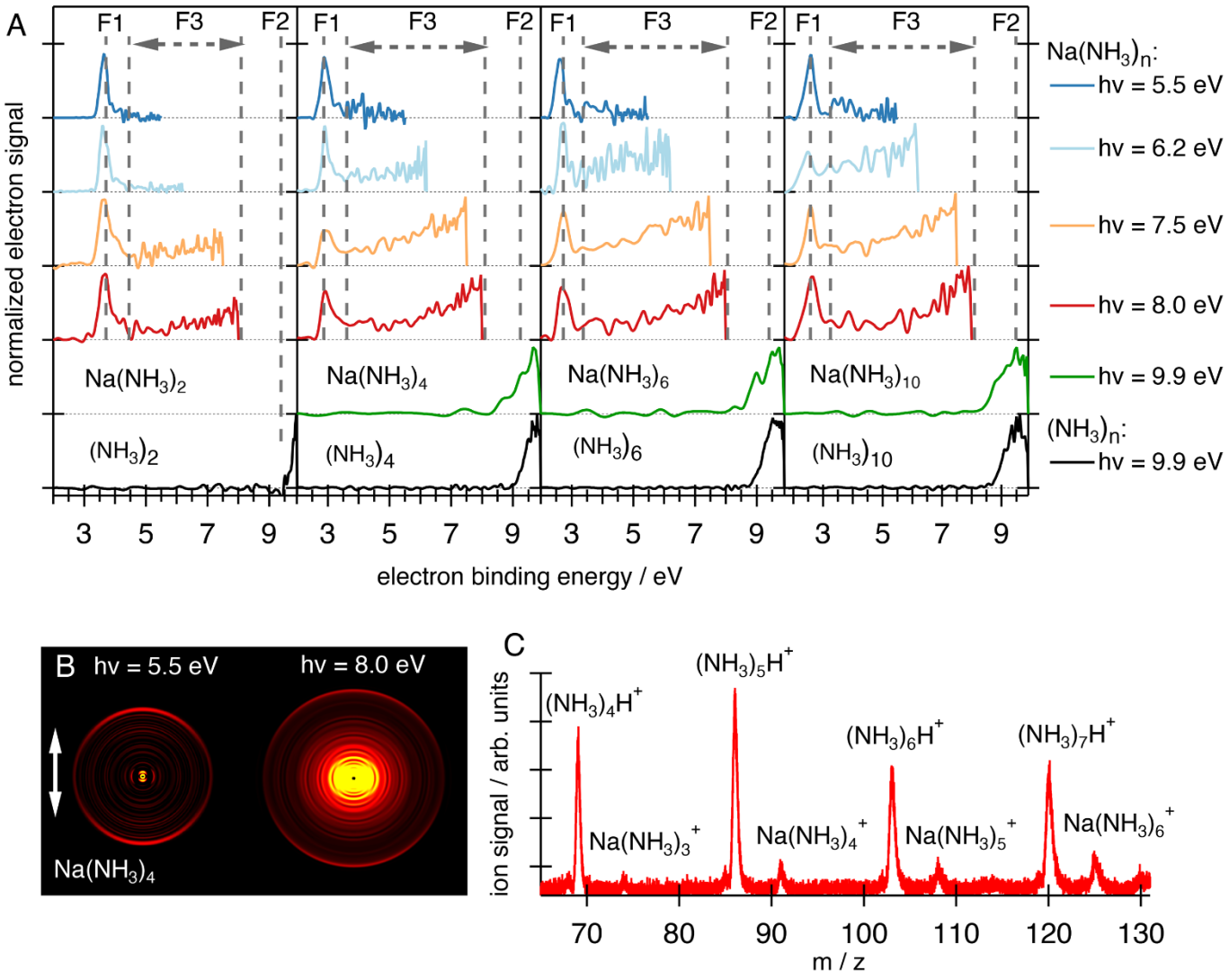

Fig. 1. Experimental results from photoelectron photoion coincidence spectroscopy of sodium-doped ammonia clusters $Na(NH_3)_n$. (**A**) Cluster size-resolved photoelectron spectra of selected $Na(NH_3)_n$ clusters recorded after photoexcitation at different photon energies $h\nu$ (dark blue to green lines). Black lines are photoelectron spectra of pure ammonia clusters $(NH_3)_n$ recorded at $h\nu$ = 9.9 eV. Feature F1: Photoelectrons from the direct photoionization of single solvated electrons in $Na(NH_3)_n$ (e^-_{ph} from Φ_{solv}, Fig. 2A). Feature F2: Photoelectrons from the direct photoionization of ammonia solvent molecules in $Na(NH_3)_n$ (e^-_{ph} from Φ_L, Fig. 2B) or pure $(NH_3)_n$ clusters (black line). Feature F3: Low-energy electrons from the ETMD of the dielectrons (e^-_{ETMD} from Φ_{solv}, Fig. 2). (**B**) Velocity map images for $Na(NH_3)_4$ recorded at $h\nu$ = 5.5 eV (left) and $h\nu$ = 8.0 eV (right). Anisotropic photoelectron angular distribution (left image) result from direct photoionization (e^-_{ph}), and isotropic distributions centered at low kinetic energies (right image) result from ETMD of the dielectrons (e^-_{ETMD}). (**C**) Section of a mass spectrum recorded at $h\nu$ = 9.9 eV comprised of intact $Na(NH_3)_n^+$ cluster signals from the pathway shown in Fig. 3B, and protonated $(NH_3)_nH^+$ signals from ionization of pure $(NH_3)_n$ clusters. Further information in sections S1 to S3.

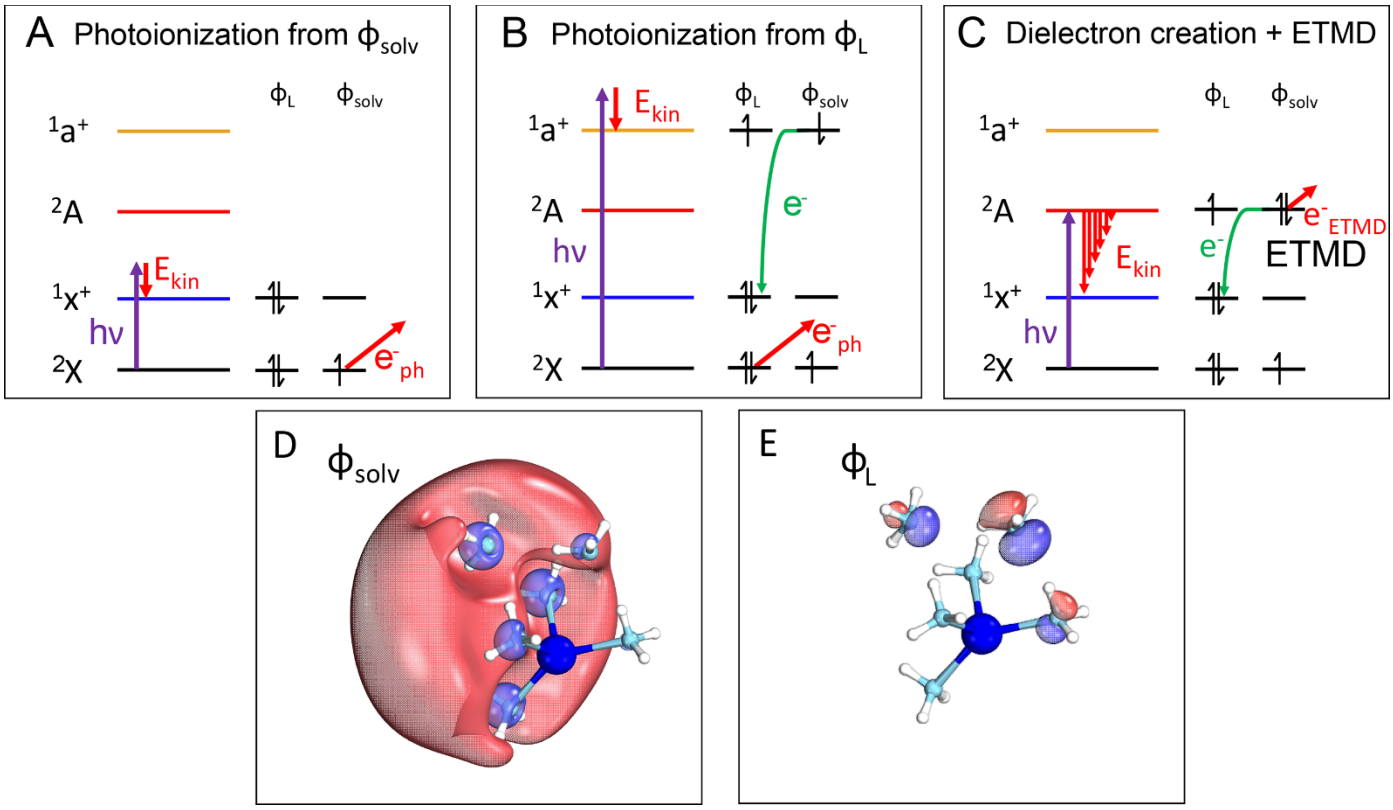

Fig. 2. The three distinct pathways of electron formation observed after UV photoexcitation of $Na(NH_3)_n$ clusters. (**A** to **C**) The three pathways. Horizontal lines on the left indicate qualitative energy levels of the four electronic states labeled ^2X, $^1x^+$, ^2A and $^1a^+$. Orbital occupations are indicated on the right. Φ_L is the HOMO of the bare ammonia solvent shell, and Φ_{solv} is the HOMO of the entire $Na(NH_3)_n$, which corresponds to the delocalized solvated electron orbital. $h\nu$ is the UV photon energy and E_{kin} is the kinetic energy of the ejected electron. e^-_{ph} (red), e^- (green) and e^-_{ETMD} (red) are electrons from direct photoionization, internally transferred electrons, and electrons from ETMD processes, respectively. Red arrows indicate the ejection of electrons, green arrows an internal electron transfer (A). Direct photoionization of a unpaired solvated electron from Φ_{solv} in $Na(NH_3)_n$ (feature F1 in Fig. 1A), producing a cation cluster in the ground state $^1x^+$. (B) Direct photoionization of an electron from Φ_L of the ammonia solvent molecules (e^-_{ph}, feature F2 in Fig. 1A) producing a cation cluster in the excited state $^1a^+$ and internal electron hopping from Φ_{solv} to the Φ_L vacancy (e^-). (C) Photoexcitation of an electron from Φ_L of the ammonia solvent molecules to the singly-occupied Φ_{solv}, forming a dielectron (^2A state). Subsequent decay of the dielectron via ETMD, producing a cation cluster in the ground state $^1x^+$. ETMD consist of internal hopping of one electron from Φ_{solv} to the Φ_L vacancy (e^-) and ejection of the second electron from Φ_{solv} from the cluster (e^-_{ETMD}, feature F3 in Fig. 1A). The electron is ejected with a broad distribution of different kinetic energies (E_{kin}, see Fig. 3). (**D** and **E**) Representation of the Φ_{solv} and the Φ_L orbital, respectively, of a $Na(NH_3)_6$ cluster (section S4).

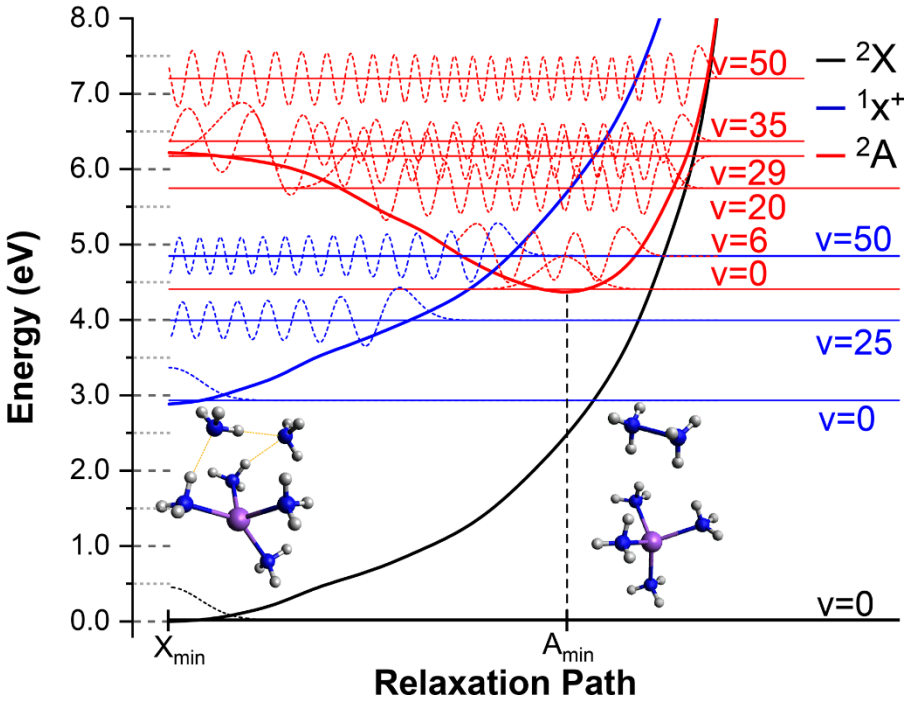

Fig. 3. Calculated potential energy profiles along the one-dimensional relaxation path of the dielectronic state for $Na(NH_3)_6$. Vertical photoexcitation from the minimum geometry (X_{min}) of the electronic ground state ^2X (black curve) creates a dielectron state in the saddle point region of the electronically excited ^2A state (red curve), which then relaxes along the path. The potential energy profiles of the ^2A state and the ground state of the cation, $^1x^+$ (blue curve), intersect before the minimum structure of the ^2A state, A_{min}, is reached. A_{min} can be described as an ammonia dimer cation $(NH_3)_2^+$ bound to a smaller sodium-doped ammonia cluster cation $Na(NH_3)_{n-2}^+$ by a solvated electron pair. Selected vibrational wavefunctions shown for the ^2X (black dashed), $^1x^+$ (blue dashed), and ^2A (red dashed) states illustrate the many possibilities (and hence the high probability) for ETMD processes to occur along the relaxation path. Further information in sections S4 and S5.

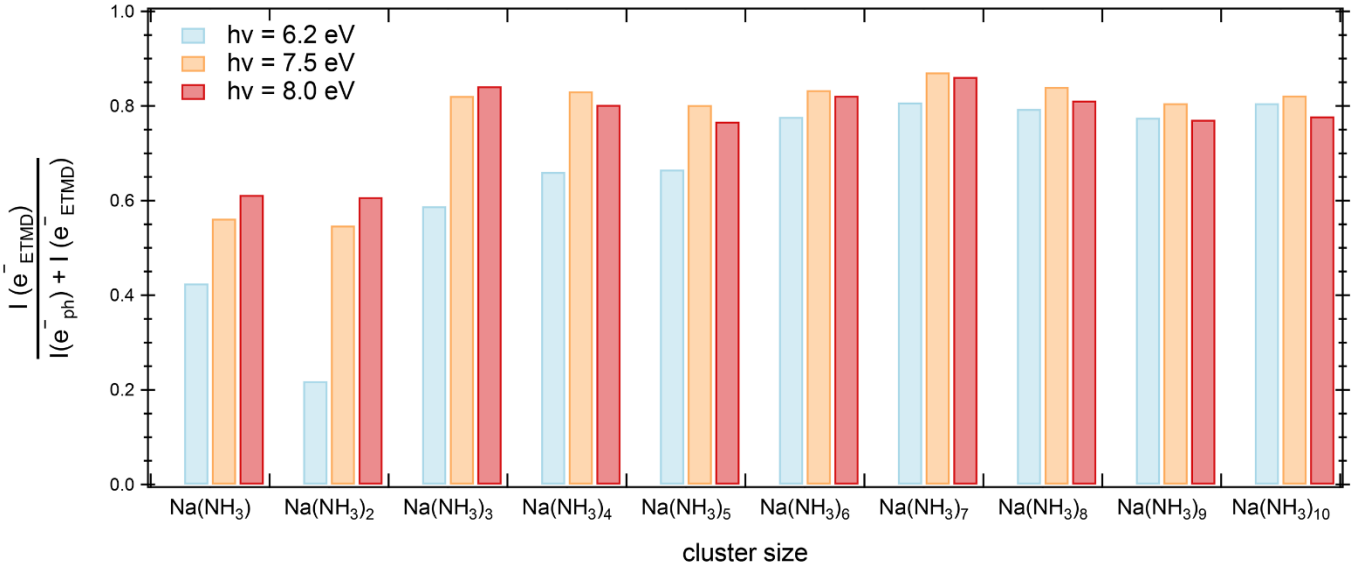

Fig. 4. Relative yield of ETMD electrons at different UV excitation energies as a function of the cluster size. Ratio $I(e^-_{ETMD})/(I(e^-_{ETMD})+I(e^-_{ph}))$ retrieved from the experimental photoelectron spectra by integrating over the F3 ($I(e^-_{ETMD})$) and F1 ($I(e^-_{ph})$) bands (Fig. 1A and figs. S3 and S4). The figure illustrates that the UV light-induced dielectron ETMD (Fig. 2C) is largely insensitive to system size and UV energy. The high relative yield of e^-_{ETMD} can be explained by the high probabilities of forming solvated dielectrons by UV photoexitation and their subsequent autoionization via ETMD (Fig. 2C and Fig. 3).

Solvated dielectrons from optical excitation: An effective source of low-energy electrons

Sebastian Hartweg, Jonathan Barnes, Bruce L. Yoder, Gustavo A. Garcia, Laurent Nahon, Evangelos Miliordos, and Ruth Signorell

Science,**Ahead of Print**
DOI: 10.1126/science.adh0184